

# Development of a new Mach 12 scramjet operating capability in the X3 expansion tube

Pierpaolo Toniato<sup>1</sup>, David E. Gildfind<sup>1</sup>, Peter A. Jacobs<sup>1</sup>, Richard G. Morgan<sup>1</sup>  
<sup>1</sup> *The University of Queensland, Brisbane, Queensland, Australia*

## Abstract

Scramjet technology is considered potentially viable up to around Mach 14, however, flight and ground tests of nose-to-tail scramjets have only been done up to Mach 10. The aim of this project is to investigate combustion in a nose-to-tail scramjet engine at Mach 12 for the first time, using the X-3 expansion tube facility, currently the only facility in the world which can reproduce the gigapascal total pressures of Mach 12 flight at suitable scales for engine testing.

This paper reports on the development of a new Mach 12 operating capability, which has required major upgrades of X3 including development of new tuned free-piston driver operating conditions, and design and commissioning of a fully instrumented Mach 12 nozzle with the aim of optimizing the test flow in X3. Preliminary experiments have been conducted in the smaller X2 facility to assess test flow noise and unsteadiness, and the performance of a different secondary driver configuration for a high density, low enthalpy Mach 13 reference condition. These experiments, reported in this paper, suggest that while the use of a secondary driver can reduce high frequency noise, it can introduce a general rising pressure gradient during the test time. However, follow-on experiments will be required in the larger X3 facility, since it is believed that part of the transient behaviour identified in the X2 flow must be attributed to the facility reduced length.

**Keywords:** expansion tube, ground testing, secondary driver, scramjet, computational fluid dynamics

## Introduction

Scramjet technology has the potential to provide air-breathing propulsion as an alternative to conventional rocket propulsion. Since the vehicle does not need to carry oxidiser, the specific impulse can theoretically be increased by an order of magnitude, thereby doubling the available payload mass fraction [1]. While scramjet propulsion is considered to be viable up to Mach 14 [2], [3], the fastest flight test was Mach 10 (NASA X43-a) [4]. At same time, ground experiment have been conducted up to Mach 10 in free-jet mode [5], and at Mach 12 in semi free-jet mode [6], [7] (i.e. assuming the test flow corresponding to the flow behind the forebody shock) in reflected shock tunnel facilities (RST).

Current ground testing capabilities are limited by the extreme total pressure requirements of above Mach 10. Total pressure requirements are further increased by pressure-length scaling, typically adopted to conserve similarity of flow between experiment and flight for the subscale model. Expansion tubes are currently the only kind of facility capable of reproducing those high-pressure requirements because total enthalpy and total pressure are added to the gas by unsteady expansion of the test gas rather than stagnating it, overcoming the structural and chemistry limitations of other kind of facilities, like RST.

This paper will outline the proposed experiments and the work already done to provide a new Mach 12 operating condition in X3. A particular challenge with expansion tubes is achieving good test flow quality and satisfactorily characterising it. Initial studies to achieve the required test flow are presented. The planned upgrades necessary to achieve the Mach 12 operating condition will be outlined in the second part of the paper.

## High Mach number scramjets

Recent study [8] observes that while there is a forecast of 130 rocket launches in the next decade, at the same time it has been estimated that approximately 1000 payloads will be launched across these 130 launches. Of those rocket launches, less than 10% are small-scale or dedicated to small systems. In this scenario these small payloads typically have no choice of orbit, necessarily adapting to the requirements of bigger and more expensive payloads. A radical technology shift towards reusable systems might represent a viable solution for lower cost and more optimal launch options for small satellites [9]. Recently scramjets have been proposed as an alternative to traditional rocket systems for powered high lift-to-drag vehicles for small payloads in 3-stage rocket-scramjet-rocket systems [1] [10].

The use of a scramjet as a second stage gives aircraft-equivalent flexibility in the launch operations if problems occur or manoeuvring around bad weather is required. Moreover, a scramjet powered stage would be inherently reusable, and able to return to the launch base [1]. In this context, a scramjet which satisfies these mission requirements would be optimally operated between Mach 5 and 12 [1].

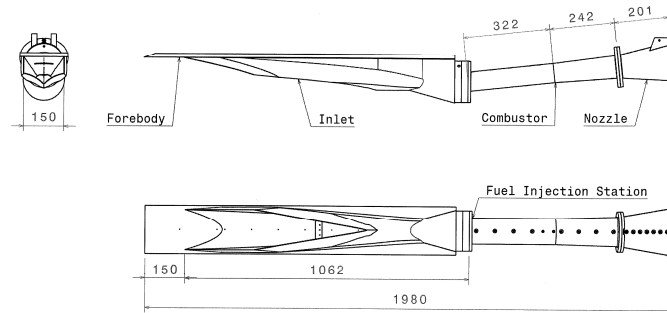


Figure 1 M12REST engine model. Taken from [4].

High Mach scramjets have been flight tested with differing results. Amongst these, as an example, the NASAX-43 vehicle achieved two successful flights at Mach 6.9 and 9.6 in March and November 2004 [4]. Flight involved a hydrogen-powered scramjet-propulsive phase of more than 5 seconds [4]. At the same time, ground testing for any kind of air breathing engine is still essential due to the costs and risks associated with flight testing. Given the remaining uncertainties relating to scramjet technology being in its early stages, and results of the previous flight test are analysed, ground testing is absolutely necessary [11].

With the goal of access-to-space-scramjet in mind, Smart developed a series of engines with a “rectangular to elliptical shape transition” REST inlet. [12]. These engines have shown strong results and the capability to operate across a wide range of conditions (see, as example, [5]). The most recent engine is the M12REST engine, which has been designed to operate a Mach 12 flight condition. The engine is shown in Figure 1 [13].

THE M12REST inlet has been tested by Suraweera and Smart [13] at full-scale but off design conditions (Mach 7.5) in semi freejet mode. A half-scale model has been tested in semi-freejet mode with a Mach 10 flow and a Mach 12 equivalent enthalpy by Wise [6] in the UQ’s T4 RST (see Figure 3). However, even though Wise tested a ½ scaled model, binary scaling was not applied, due to limitations of the T4 facility in terms of stagnation pressure and temperature. Flow density could not be increased further to maintain the pressure-length product of the full-size flight vehicle.

Doherty [5] developed a streamlined, airframe integrated M12REST engine at 0.32 scale with respect to one designed by Suraweera [13], in order to fit the whole model into the core-flow of T4. Doherty’s engine (see Figure 2) has been tested in freejet mode at Mach 10 for an equivalent dynamic pressure of 28 kPa, with the use of multi-component force balance [14]. Similarly to the Wise tests, no pressure length scaling was applied.

The pressure length scaling required to test the M12REST engine at flight condition are not only out of the operating range of the T4 RST, but also out of the range of all RST, like HIEST or LENS I/II. [15] [16], because in these kind of facilities the high speed flow is obtained by first stagnating the test gas at the required total pressure. This is a fundamental limitation of RST facilities which cannot be significantly addressed through improved design and materials. Expansion tubes, as we will see in the following section, allow this limitation to be overcome. The tests of these engines at matched design/flight conditions provides the motivation for this study.



Figure 2 M12REST engine 0.32 scale, attached to multi-component force balance. From [14].



Figure 3 M12REST engine half-scale model. From [6].

### Expansion tubes

The expansion tube derives from a generic shock tube with the addition of a low pressure section after the shock tube (called acceleration tube), with the two sections separated by a thin secondary diaphragm. The schematic of an ideal expansion tube is shown in Figure 4. The test gas, which is contained in the shock tube, is first processed by a normal shock wave generated by the rupture of the primary diaphragm, which is typically made of aluminium and ruptures at high pressure.

The secondary diaphragm is subsequently ruptured upon impact of the shock wave that has in the meantime shock-processed (i.e., accelerated and heated) the test gas. The incident shock waves continues its path along down the acceleration tube, where the gas is highly accelerated and heated. Behind this shock wave the test gas, already set

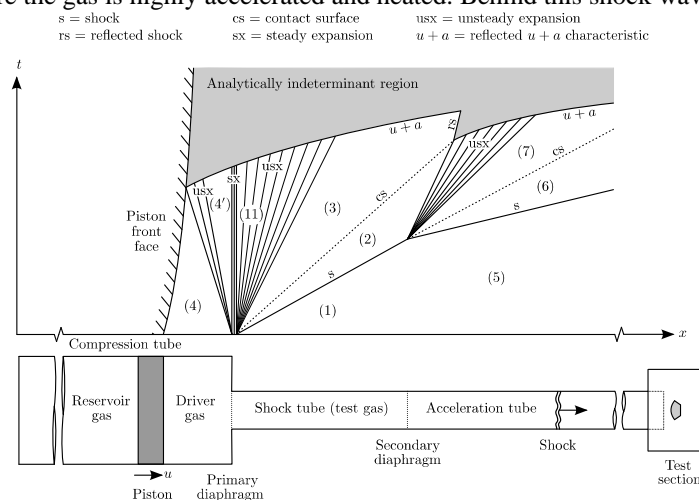


Figure 4 Ideal  $x-t$  diagram of a basic expansion tube, without secondary driver. Adapted from [28].

in motion by the shock itself, expands into acceleration tube by mean of an *unsteady expansion*, which is the fundamental phenomenon involved in the generation of an hyper-velocity flow in an expansion tube. The gas may finally be expanded to the desired Mach through the use of a hypersonic nozzle. The main advantage of expansion tubes is the unsteady expansion mechanism, which increases the total enthalpy and total pressure of the flow without stagnating it [17].



Figure 5 Mach 10 2-D Scramjet inside the X3 expansion tube. Side covers are removed showing the internal instrumentation.

### UQ's expansion tubes

UQ currently operates two free-piston driver expansion tubes, X2 and X3. Both use a piston to compress and subsequently heat the driver gas to very high pressures and temperatures. The X2 expansion tube is a medium size facility and which was commissioned in 1995. It has a total length of 23 meters. Its 9m long, Ø85.0mm diameter driven tube, which can be fitted with a full capture and shock free Mach 10 nozzle [18], can be internally partitioned in two (as in Figure 4) or three sections using thin diaphragms made of film materials such as Mylar or aluminium. Each section contains volume of gas of different composition and pressure, chosen such as to obtain the desired flow condition at the end of the acceleration tube, where the tube is connected to a large-volume dump tank, and where the model is located.

X3 is a larger version of X2 in University of Queensland, and theoretically has the highest performance in term of total pressure and total enthalpy amongst all expansion tubes in the world. The total length is 70m, with a 14.5 m long compression tube. The acceleration tube diameter is 183mm and its current Mach 10 nozzle has an internal exit diameter of 440mm. Currently, X3 is the only facility in the world which can theoretically reproduce the gigapascal total pressures of Mach 12 and above flight for model sizes up to Ø 300 mm and sufficient test time (~1ms). The facility is similar to X2, with a driven tube divisible in two or three sections, a Mach 10 nozzle and a dump tank in which models are located. In Figure 5 a Mach 10 2D scramjet inside the X3 test section is shown.

Both X2 and X3 facilities have been used to do scramjet testing. McGilvray et al. [19] tested a nose-to-tail scramjet for the first time in an expansion tube; it was a 2/5 scaled 2D hydrogen-fuelled scramjet derived from an existing scramjet tested in the T4 RST. The engine was tested in X2 at Mach 10.1, 165kPa equivalent flight dynamic pressure for a test time of 400 $\mu$ s. Sancho [20] tested the corresponding full-scale Mach 10 scramjet (see Figure 5), matching the condition developed in T4 (Mach 10, 65kPa). Within the same study, he tested the engine with a 190kPa dynamic pressure condition, for an equivalent total pressure of more than 1Gpa. Those tests, and their comparison with results from T4 have shown good agreement, considering the experimental uncertainties. This was considered a validation of X2, X3 and expansion tube in general for scramjet testing.

### Characteristics of expansion tube test flows

Expansions tubes, while being able to produce the highest enthalpy and highest total pressure of any type of wind tunnel facility, are characterized by some peculiar features, like short test times, flow unsteadiness and acoustic disturbances in the test flows. An additional section, named secondary driver, can be added to the facility to increase its performance [21]. These characteristics will be described in the following sections.

#### Test times

Expansion tubes, along with all others kind of impulse facilities are limited by the amount of test time that they can provide. For this kind of facility, the test gas is usually limited either by the arrival of the contact surface between the driver gas and test gas or the reflected head of the unsteady expansion originated at the secondary diaphragm, as shown in Figure 1. This is critical for scramjet flow processes where flow establishment times are of the same order of magnitude of the test time. However, McGilvray showed that the initial flow of acceleration gas through the engine can lower these requirements [22], allowing the engine to start at the lower pressure of the acceleration gas. The use of relatively long facilities, like X3, are necessary to achieve significantly longer test times (1-2 ms) compared to X2.

#### Flow disturbances

Initial developments indicated that expansion tubes would be able to simulate a wide range of conditions [23]. However, many flow conditions had unacceptable levels of noise, making the conditions useless using the Langley Expansion tube [24], such that only a narrow range of suitable test flows could be achieved.

Paull and Stalker [25] later investigated the operation of a free piston driver expansion tube to understand the cause of the flow disturbances that limited the amount of test gas that was sufficiently steady to be usable. It was determined that the unsteady expansion is responsible for the transmission of the noise through the test gas. Indeed, it produces a large drop in the sound speed of the test gas, which has the effect of focusing the different components of the frequencies of lateral acoustic waves into a narrow band of frequencies, that later appear as disturbances in the test gas.

The same authors postulated that the main source of the noise (later identified in the test flow) originates during the primary diaphragm rupturing process. They subsequently found that penetration of the acoustic waves can be inhibited by configuring the expansion tube in an over-tailored configuration, i.e. such that the speed of sound of the expanded driver gas is lower than the speed of sound of shock processed test gas.

They proposed a tailoring ratio of  $a_2/a_3 = 1.25$  to achieve an "acoustic buffer" and prevent the noise from propagating through into the test flow. Such a value for the ratio has been supported experimentally [17]. A simple and clear example can be seen in Figure 6. The accelerator gas, initially at a very low pressure, is processed by

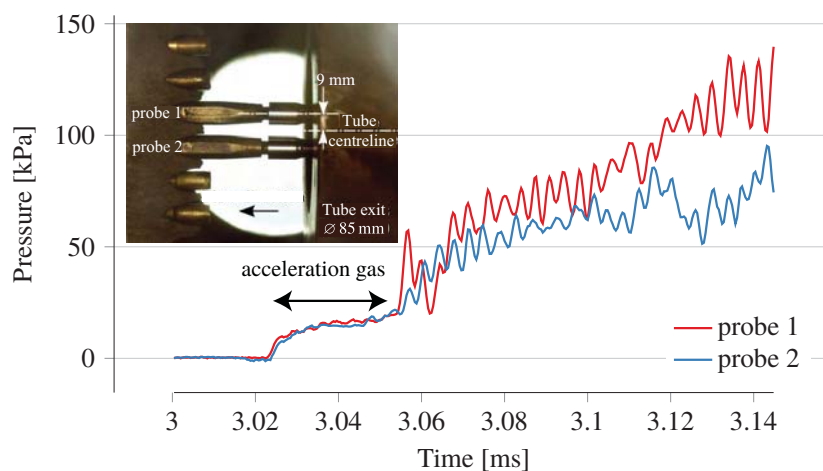


Figure 6 Cone probe impact pressure measurements. Acceleration gas passes the transducer between the first and the second rise of the trace that corresponds to the arrival of the noisier test gas. Shot x2s2756, Mach 13 scramjet condition.

the shock wave after the rupturing of the diaphragm, and its sound speed becomes higher than that of the test gas. Therefore, the interface supposedly acts as the acoustic buffer filtering all the radial waves that are clearly present in the test gas.

### Secondary driver

A secondary driver is an additional section that can be interposed between the driver and shock tube. Firstly proposed by Henshall [26] it was tested experimentally for the first time by Stalker and Plumb [27] in a shock tube facility to drive stronger shocks. Several years later, it was implemented in an expansion tube to achieve superorbital test flow shock speeds, up to 18.7km/s [21].

To enable this mode, an additional film diaphragm is inserted; the secondary driver is separated from the primary driver on one side by the primary diaphragm, and shock tube on the other side by the secondary diaphragm. This section, filled with helium, while being located in the driven tube, becomes the effective driver gas for the test gas in the shock tube. The shock generated by the rupture of the primary diaphragm processes the secondary driver helium, increasing its temperature, pressure and flow speed. Indeed, it can be shown [28], that given a low enough pressure helium gas, the shock-heating will raise the temperature such that the speed of sound of the shock-processed secondary driver is higher than that of the primary driver. Given the strong dependence of shock speed on driver gas sound speed, this results in the capability of the secondary driver to generate a stronger shock through the test gas compared to what could be achieved by the primary driver alone. This performance increase represented the motivation for the initial studies, as explained in detail by Morgan [29]

This performance increase, however, comes at the cost of reduced test time. This occurs for two reasons: the flow processes that this mechanism can support are reduced, and second, for a fixed tube length, the presence of a secondary driver reduces the length of the shock tube therefore by reducing the available amount of test gas.

The normal operating mode of a secondary driver which produces a performance increase is when an unsteady expansion at the secondary diaphragm is produced [28]. However, if the test gas has a sufficiently high density compared to the secondary driver gas, which is the case for scramjet conditions with respect to the secondary driver gas, the shock-processed gas must slow down instead of expanding when hitting the test gas. Then, instead of the targeted unsteady expansion, a reflected shock originates at the secondary diaphragm [28].

### Secondary driver as acoustic buffer

Scramjet conditions are relatively slow and high density (3-4 km/s) compared to the planetary re-entry (10 km/s) that have been traditionally produced in expansion tubes. They fit into the category of low enthalpy condition as defined by Paull and Stalker [25], who proposed that such conditions cannot be simulated with satisfactory test quality. Morgan [29] however, noted that the required sound speed increase could be obtained by using a helium secondary driver. Indeed, it could be easily configured in over-tailored mode to obtain a sound speed higher than that one of the expanded driver gas. The disturbances generated by the flow across the primary diaphragm area change are then theoretically suppressed by the shock-processed helium gas. Nonetheless, the work done by Morgan [29] did not take into account the reflected shock waves that arises at the secondary diaphragm. Indeed, the acoustic effects on these waves over the test gas in presence of a secondary driver with reflected shock are yet to be assessed, and form the central scope of this paper.

### Test flow unsteadiness

It has been noted by McGilvray [22] and Sancho [20] that scramjet conditions in expansion tube are also characterised by the undesirable feature of a steadily rising gradient that can be observed in the Pitot pressure traces (in addition to the flow disturbances already illustrated in the previous sections). As an example, the phenomenon can be observed in Figure 6 in the test gas. McGilvray elaborated and validated a technique, named slug-tracking, for analysing quasi-steady scramjet measurements [30], allowing experiments presenting this undesirable feature

*Table 1 Initial fill conditions of X2 experimental campaign. All use primary driver operation condition x2-lwp-2.0mm-100He-0 (See [28]).*

	$p_{sd1}$ [Pa] He	$p_1$ [Pa] Air	$p_5$ [Pa] Air
3a	1000	14330	1.09
3b	10000	83820	6.35
3c	50120	232500	17.57
3d	398100	548200	41.33
3e	N/A	548200	41.33
3f	1000	548200	41.33
3g	10000	548200	41.33
3h	100000	548200	41.33

to be evaluated and normalized. However, the origin of this phenomenon has not been identified, and additionally its interaction with the use of a secondary driver remains to be studied.

### Experimental and numerical investigation

Acoustic disturbances and flow unsteadiness represent a substantial obstacle towards the full characterization of test flows in expansion tubes. The plan to develop a new Mach 12 condition for X3 requires addressing the lack of specific study about these phenomena and the effects of the use of a secondary driver. It has been considered useful to undertake an experimental investigation in the smaller X2 facility to explore further.

However, in an expansion tube it is very difficult to measure the flow properties directly without the use of intrusive system of measurements. As an example, static pressure can be measured along the tube wall, but it cannot be characterized inside the core flow without interfering with the flow itself. A numerical study is therefore complementary to expand the set of information available to the experimenter. Full facility CFD simulations are computationally extremely expensive due to the size of the facility itself, the necessity of fully resolving the transient features of the flow, and the chemistry associated with high temperature of the gas.

For the present study, both experiments and CFD studies of the smaller X2 facility have been conducted for a set of Mach 13 reference scramjet conditions illustrated in Table 1. X2 for these experiments has been operated without a nozzle, in order evaluate the acoustic effects without the added complexity introduced by the nozzle expansion.

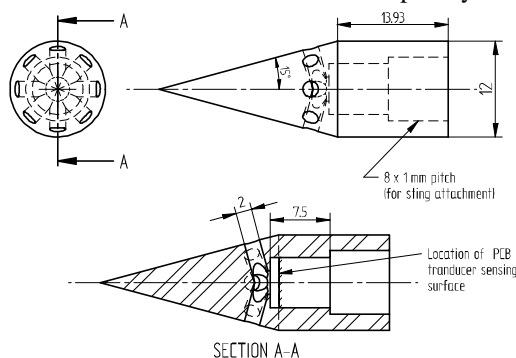


Figure 7 Schematics of 15 deg half-angle cone probe. All dimension in mm. From [31].

Static pressure measurements were taken at different locations along the driven tube. These measurements are useful to indicate the shock arrival time and to evaluate the shock speed between the transducers, for comparison with CFD simulations.

Experimental Pitot pressure measurements are the primary mean to identify the test time, flow steadiness core flow size. However, expansion tube are extremely taxing over the pressure sensors because of the high pressures and elevated temperature flow. Additionally, a large amount of Mylar film are used for the diaphragms to resist high initial fill pressures, such that, once entrained in the flow, can damage the pressure sensors. In order to reduce the damage, conical probes have used to measure the flow in the test section. The probe consists of a 15° half angle cone, with 8 perpendicular holes supplying the pressure sensor transducer cavity. Details of this cone probe pressure can be found in [31]. The resulting pressure is not equivalent to the Pitot pressure that would result from a classical blunted probe, and correlation factor with CFD are necessary, in order to recover the correct, theoretical pressure. However, for those high Mach number, the Mach number independence principle hold, such that the ratio between the pressure registered by the conical probe and the one registered by a Pitot probe is fairly constant. For these experiments, two probes were located at the tube exit and centred about the tube centreline, as shown in Figure 6.

### Numerical models

The Eilmer3 code, developed at the University of Queensland by Jacobs and Gollan [32] has been used to perform the axi-symmetric full facility simulation. The code currently does not implement moving mesh for the free piston driver, so that an equivalent fixed volume driver has been used to simulate the volume between piston and primary driver. Initial conditions of the fixed volume driver have been calibrated such that the shock speed in the following driven tube would closely match the experimental results, as explained in detail by Gildfind et al. [33]. The X2 facility has been modelled as a two-section cylindrical model, in which the first section represent the fixed volume piston driver and the second represents the driven tube in all of its length (9.105 m). A final section to model the dump tank is added in which the flow is free to expand. The simulations are compressible, transient, viscous and turbulent (Baldin-Lomax). Two meshes have been prepared, with 210000 and 520000 elements with 40 elements in the radial direction, and a radial clustering towards the tube wall.

The primary diaphragm has been modelled as a gradually opening diaphragm in which the area increases linearly over time, with a total rupturing time equal to 167  $\mu$ s [34]. While the actual opening process is non-ideal and only sophisticated investigation would be able to characterise the real rupturing process, numerical studies [35] have shown that a basic iris-model is sufficient to capture complex flow features. Secondary and tertiary diaphragm models assume a fully opened diaphragm after a hold time of 10  $\mu$ s, considering that the real diaphragms fragment and vaporise after the shock arrival [36]).

It is expected that this model, that includes the area change and a gradually-opening diaphragm, would be able to create flow disturbances at least characteristically similar to the ones that, according to Paull and Stalker [25] are generated through the unsteady expansion of the driver gas through the rupturing primary diaphragm and across the driver area change.

Conical probes have not been included in the full facility simulations, opting for a 2-step approach: the flow field properties in the location of the head of probe from the full-facility simulations have been extracted and a 2D simulation of the flow over a 15° cone has been carried out. The static pressure has been extracted from the point on the cone surface corresponding to one of the hole feeding the transducer cavity. To validate this approach, the same transient inflow condition has been used to evaluate the flow behind an ideal cone using the Taylor-Maccoll equations, coupling it with CEA [37] to include equilibrium gas effects. The flow resulting from this calculation has been compared with the 2-step CFD results and very good agreement has been observed.

A complementary model with a quasi-one-dimensional Lagrangian code, L1d [38] has been prepared and simulated, to further validate the CFD simulations. The model used for those simulation is identical to the CFD one, using a fixed-volume driver. Diaphragms in L1D have been considered ideal with zero mass. Contrary to the CFD, no viscosity model have been used.

## Results

Figure 8, Figure 9, Figure 10 show the shock speeds calculated from the CFD simulations, L1D and experimental results for the three different conditions that have been tested and simulated (3e, 3d, 3c from Table 1). Experimental shock speeds are calculated between two adjacent transducers in the same tube. Numerical shock position have been extracted from the result, detecting the initial step pressure rise associated with the shock arrival at every time step. Shock speed are then obtained by differentiating the shock position.

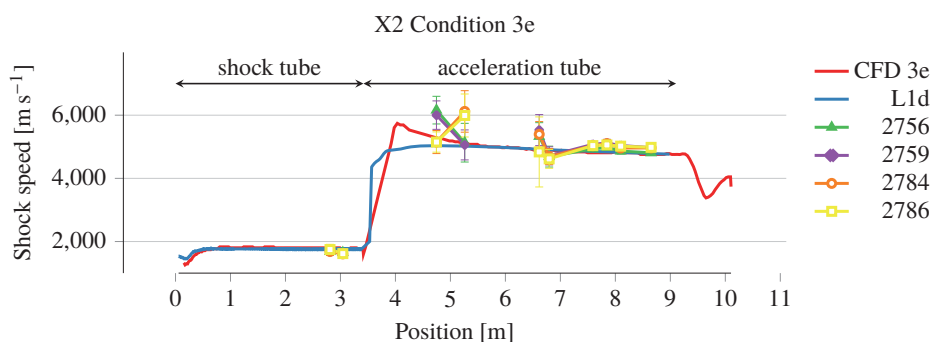


Figure 8 Experimental and numerical shock speed vs position for condition 3e, without a secondary driver.

For condition 3e (no secondary driver), Figure 8, the calculated experimental shock speeds are on average less than 3% different to the estimate given by both the numerical tools. The discrepancy between L1D and Eilmer3 shock speeds after the tertiary diaphragm are explained by a slightly different opening model for the diaphragm. The dip in the shock speed (common to all the simulations) after 9.1 m is due to the expansion into the dump tank.

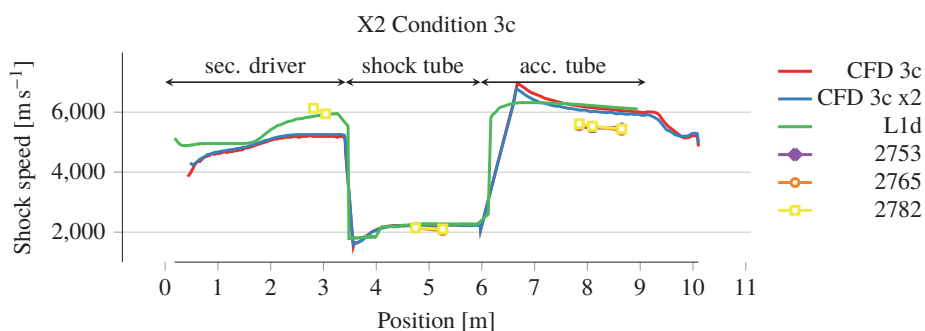


Figure 9 Experimental and numerical shock speed vs position for condition 3c, with sec. driver.

The introduction of the secondary driver for the other two conditions change the predictive ability of the numerical tools. In Figure 9, in the secondary driver there is good agreement between L1D and the experiment, with Eilmer showing a larger discrepancy. This difference has already been observed in other simulations for different conditions ([34]) and it can be explained by the smearing of the re-compression wave through the diaphragm opening, which is accurately modelled by L1D. It is clear that the inclusion of a full piston model would be helpful to increase the fidelity of the CFD simulation. The code successfully reproduces the drop in shock speed through the secondary diaphragm, with good agreement with experimental results. The difference between experimental results and numerical result in the acceleration tube is over 20% and that cannot be explained by a modelling error, as the exact same model (with the exception of the secondary driver) has been used for all tubes and all flow conditions. Figure 10 presents similar results: good agreement for the secondary driver and shock tube, with great discrepancy in the acceleration tube.

Despite significant analysis, the cause of these discrepancies are yet to be identified, some hypothesis have been proposed. The consistent difference between condition 3e and 3c/3d is the presence of a secondary driver, which allows for a relatively short acceleration tube. It is postulated that the test flow in these condition behaves in a fundamentally different way, strongly influenced by shock establishment processes and interface mixing phenomena. Indeed, the short tube length is thought to amplify non-ideal flow processes. Additionally, the tertiary diaphragm in the experiments consisted of several layer of Mylar, (up to seven), such that the rupture mechanism is probably highly non-ideal.

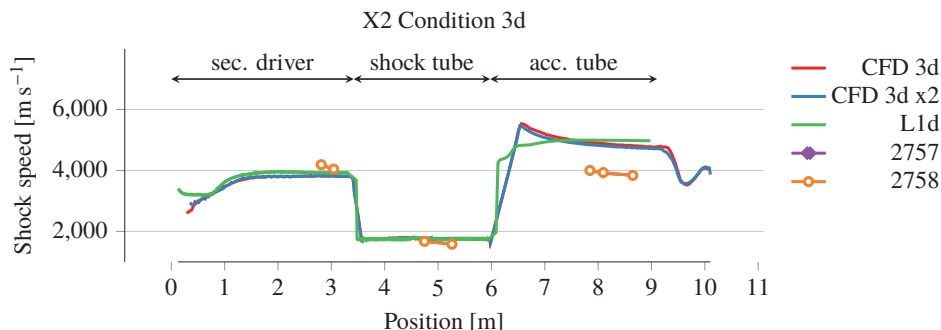


Figure 10 Experimental and numerical shock speed vs position for condition 3d, with sec. driver

### Static pressure traces

In Figure 11 acceleration tube static pressure traces are shown for condition 3e. Experimental signals have been filtered with a moving average over a window of  $10\mu\text{s}$ . The numerical results shown for these figure are taken from the higher density mesh simulations. There is excellent agreement between the different experimental traces for each condition, especially for the immediate flow following the shock arrival where the traces express the same in-phase disturbances. CFD results shows good agreement to the mean value of experimental data, confirming the correct shock speed results of Figure 8. The dip that is observed  $50\mu\text{s}$  after of the shock arrival is due to the passage of the bulge created by the boundary layer development. The different duration of the dip compared to the experimental results is probably due to an insufficiently refined grid. For these condition, it is difficult to identify a steady section of the pressure trace that would correspond to the test time.

CFD results for condition 3d and 3e shows a comparable behaviour and do not match the experimental results. The shock-processed CFD static pressure is higher than the experiments, which is consistent with higher CFD shock speed, as expected.

Condition 3e static pressure traces

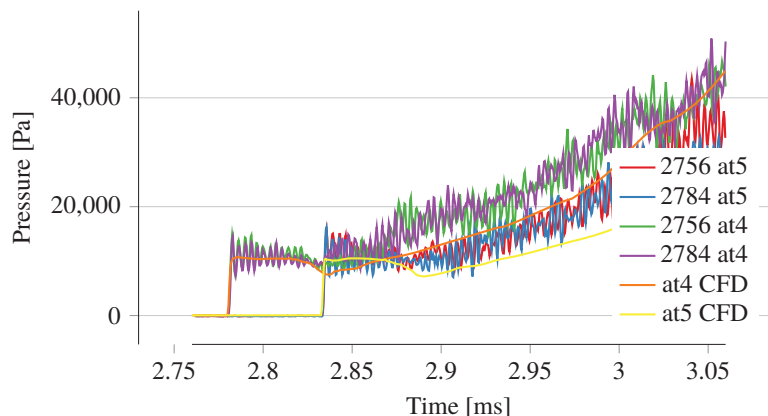


Figure 11 Acceleration tube static pressure traces: at4 and at5 sensors (located at 7.509m and 7.7846m from primary diaphragm) and comparison with 2D CFD simulations. All traces have been time referenced such that the pressure increase due to the shock arrival are coincidental.

### Test flow properties

The properties of the test flow have been evaluated experimentally through the use of four cone pressure probes and numerically with the use of the two steps simulations detailed in the previous sections. The results are shown in Figure 12. All traces have been time-referenced and centred over the pressure rise associated with the arrival of the acceleration gas-test gas interface. Experimental signals have been filtered with a moving average over a windows of  $10\mu\text{s}$ .

There is a substantial difference between the simulated cone pressure and experimental results, as shown in Figure 12 for both conditions. This discrepancy for condition 3d and 3c is related to the prior difference in the shock speed estimation, implying a lower Mach number and therefore a lower experimental cone pressure. However, condition 3e, without secondary driver, have shown good agreement both in terms of shock speeds and static pressure levels.



It is supposed that the current numerical model for the conical probe is lacking necessary modelling fidelity. Indeed, while similar models have shown for slower (Mach 10) condition a certain degree of agreement [34], the results indicate that experimental cone pressure measurements are not well matched. A possible explanation is that the probe dynamic response time is comparable to the phenomena being measured, entraining a resonant, non-linear response. Additionally, as already noted for equivalent blunted pressure probes [39], the probe could behave as a Helmholtz resonator. Further experimental and computational analysis is necessary in order to assess the response of these cone pressure probes.

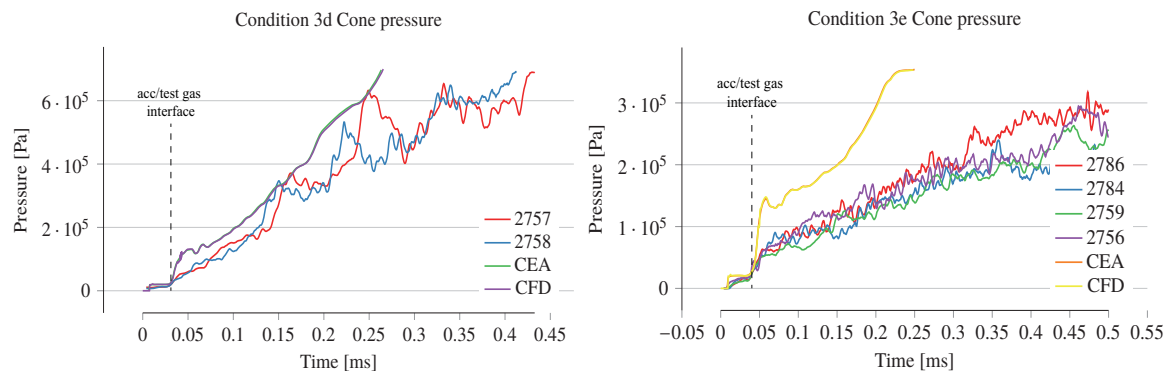


**Figure 12:** Cone pressure probes traces for condition 3d and 3e (no secondary driver) compared with 2D CFD data. CEA line calculated with Taylor-Maccoll equations coupled with CEA, to include real gas effect.

Additionally, it is difficult to observe and identify any clear test time for the conditions. Qualitatively we observe a reduction in high frequency flow disturbances with the use of a secondary driver, but there is a significant steady rising pressure gradient. Mixing phenomena in the shorter X2 facility might be responsible for the lack of available test time, and also explaining the difference between the experimental cone pressures and the numerical ones.

Considering the numerical results, it is additionally clear that there is a total absence of noise or flow disturbances with respect to the average flow in the static pressure traces and in the cone probe pressure traces. Further investigations showed that Eilmer3 uses a specific spatial reconstructor scheme in which the new interpolation values lie within the range of the original cell-centred values. While it increases the stability of the code, it has the side-effect of filtering high frequency noise, which was the goal of this study.

### Effect of different secondary driver filling pressure

In Figure 13 cone pressure traces are shown for the same shock tube and acceleration tube pressures, and increasing secondary driver filling pressures. Data has been initially presented in [28], but it is further analysed here for relevance to the noise problem.

In the first subfigure, without a secondary driver, the flow is steadier, with an eventual quasi-steady test region from 3.55 to 3.65 ms. In this case oscillations of 10% over the average flow can be observed.

On the other hand, it is very difficult to identify a suitable test time in any of the conditions that used a secondary driver, where a steady increase in the pressure trace is observed. The secondary driver seems potentially to be effective in reducing the high frequency disturbances in the test flow, but at the price of greatly reducing the macroscopic quality of the condition. Additionally, there is no qualitative difference between different cases for secondary driver in terms at different filling pressures.

It is important to note that while the use of a secondary driver reduces the high frequency disturbances, it introduces a highly non-ideal response of the test gas, so its final effectiveness is questionable. A similar qualitative steady pressure gradient has been observed in X3 (see [20]), which could be explained by the presence of a secondary driver.

### Summary

The initial use of X2 as a more manageable proof of concept has shown drawbacks: the conditions tested have shown the performance limits of the facility. In these high density, high Mach number tests a sufficiently steady test time could not be identified. Numerical results have shown partial agreement with the experiments, but discrepancies were found in the cone pressure traces. Mixing interface phenomena and highly non-ideal diaphragm rupturing processes, in combination with insufficient tube length, are thought to be responsible for the discrepancies. The use of a secondary driver did not show a substantial enhancement in flow quality to justify its use for these conditions, but the above discrepancies leave the question unanswered.

These findings will be reported and applied to the X3 expansion tube. Mixing phenomena and non-ideal processes are expected to be less significant because of the longer tubes and test times (1ms), and the bigger core flow.

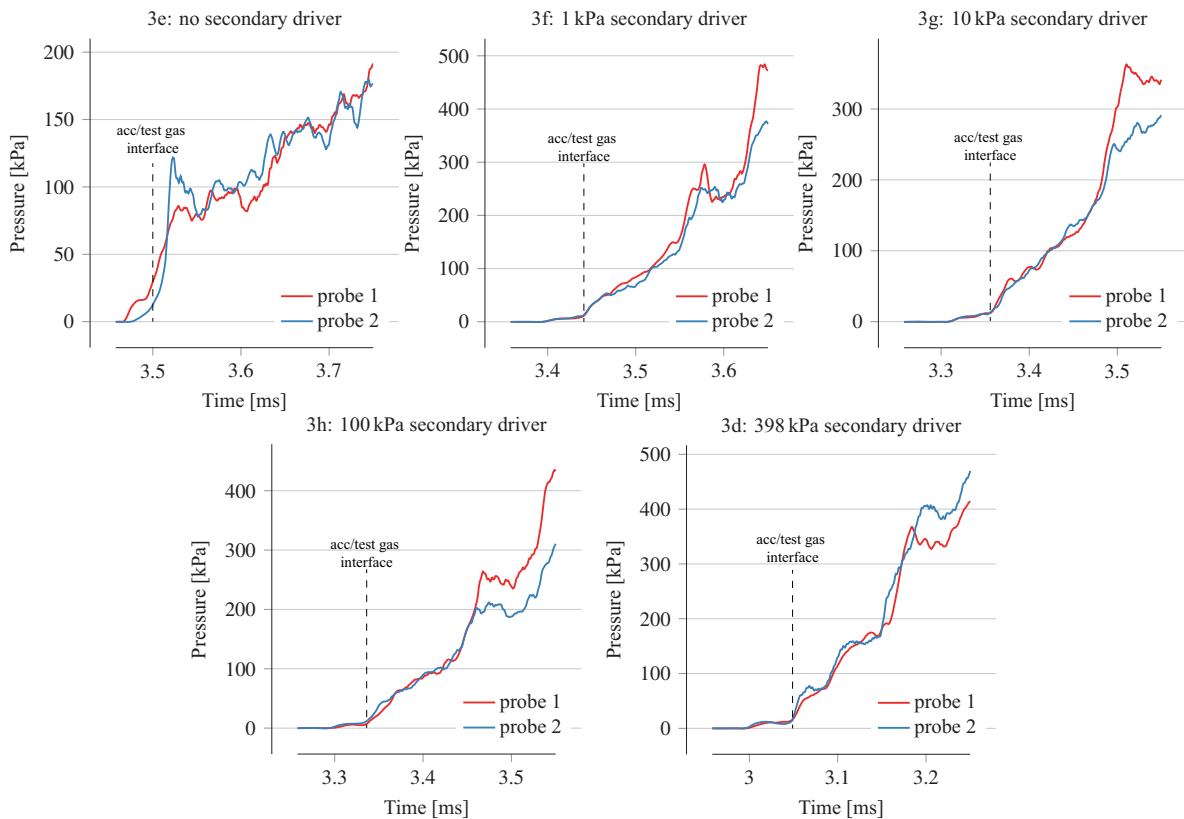


Figure 13: Impact cone pressure traces at different secondary driver filling pressures. Adapted from [28].

### X3 facility condition development

The X3 expansion tube is currently fitted with a heavyweight piston (200 kg) first commissioned in 2010 by Dann et al. [40], and a Mach 10 nozzle designed by Davey [41]. In this configuration the facility has been extensively tested and proven to be able to generate Mach 10 scramjet conditions reliably [20]. New upgrades are current planned and being developed both to increase the performance for high enthalpy conditions and to increase flow Mach number. Additionally, X3 will be configured to be allow operation in reflected shock tunnel mode [42]. These upgrades will be detailed in the following sections.

#### A lightweight piston

The current piston is not able to produce high enthalpy test flows (10-15 km/s) because tuned operation of the current piston can be achieved with large mass fraction of Argon, with a low sound speed. To achieve the desired conditions an increase in the speed of sound is necessary. To tuned the piston at those conditions a lower piston mass is then required. A new lightweight piston (100.8 kg) has been developed for X3 (see Figure 14) [43]. Initial commissioning in 2013 indicated that X3 current reservoir would not achieve sufficient piston speeds for tuned operations and a new reservoir extension have been manufactured to increase its total volume, finally allowing lighter piston speed and increasing the maximum fraction of helium in the primary driver, to further increase the flow condition envelope of the expansion tube.

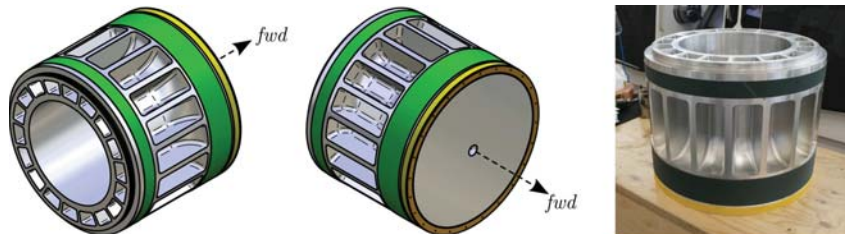


Figure 14 X3 Ø500 mm lightweight piston, 100.8kg, 6061-T6 alloy. From [43].

#### X3 in reflected shock tunnel mode

Morgan and Gildfind [42] investigated the possibility of a new operating configuration for X3 as a reflected shock tunnel for lower speed conditions in the equivalent flight regime of Mach 5 to 8. The larger internal diameter (182.6 mm) and X3's length will potentially allow for test times in the order of 10's of milliseconds. Two new nozzles, for Mach 5 and 7 flows, will be of considerable diameter (up to 800 mm). Initial modifications are underway, with

a new dump-tank extension that will internally house the nozzles, thereby reducing the pressure force over their external surface.

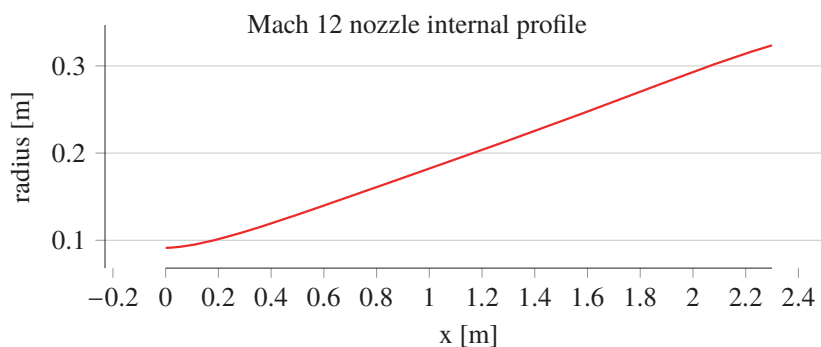


Figure 15 Mach 12 nozzle internal profile. Adapted from [44].

### Mach 12 nozzle

While the two previous sections illustrated some concurrent modifications of the X3 expansion tube not strictly related to the development of a new Mach 12 operating condition for scramjet testing, the planned new Mach 12 nozzle is of central importance. The nozzle contour has been optimized by Wei et al. [44] and the results obtained are summarized here. An initial nozzle was calculated with an inviscid method-of-characteristic code, adopting a nine Bezier control point model for the nozzle profile. A Nelder-Mead optimization process was then used with Eilmer3, in space-marching mode, to evaluate the performance with viscous effects. The chosen objective function minimizes the error variance against design Mach number and flow angle, using additional penalty function to avoid the formation of shock waves in the nozzle and to reduce nozzle centreline disturbances. Detail of the nozzle contour are shown in Figure 15. The nozzle profile, initially 2.8 m long has been finally truncated by 0.5 m, noting that the change in slope in the final section contributes little to the straightening of the flow. Additionally, the boundary layer growth and the consequent further reduction in smaller core area eliminates the already small beneficial effect of that section. The final nozzle profile is shown in Figure 15.

In the mechanical design process, currently underway, the nozzle will integrate the planned modifications of the X3 expansion tube, and as such, it will sit inside the dump tank extension. This will allow for a smaller and better sliding sealing surface between nozzle and test section, allowing for increase low pressure capability of the facility. The nozzle will be fully instrumented, with pressure gauges and heat gauges that will allow for detailed experimental comparison of CFD simulation of the nozzle flow. The nozzle inlet would be designed to host an instrumented pitot rake, in order to further increase the capability in terms of flow characterisation. Together with a classical rake at the exit of the nozzle, it will permit evaluation the effect of the nozzle on the quality of the test flow and its influence in term of test time. The new test section assembly is shown in Figure 16.

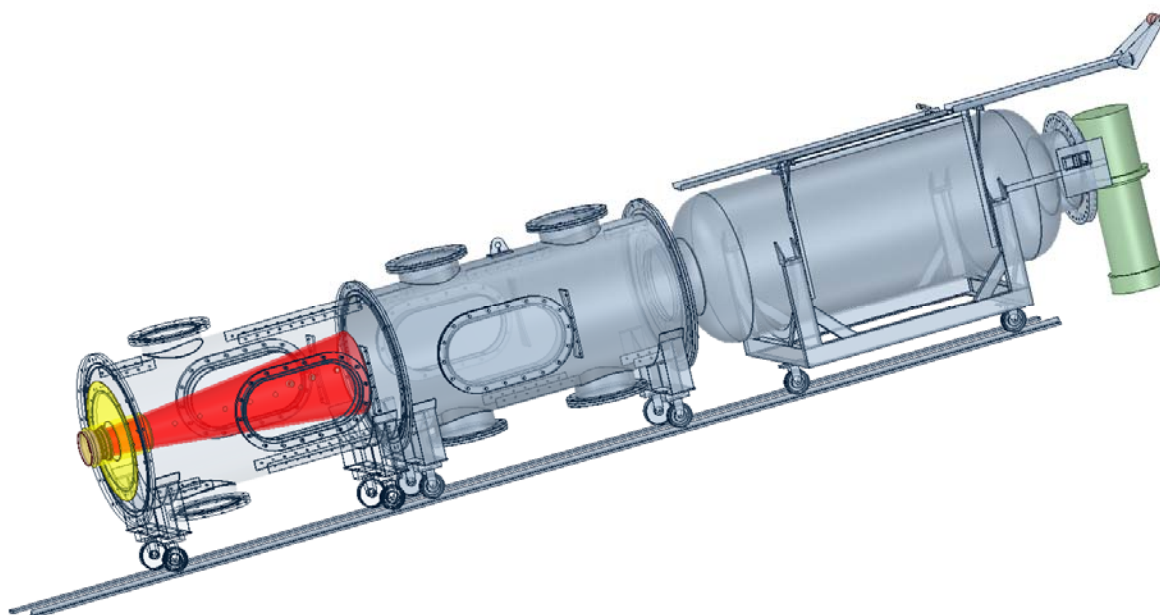


Figure 16 Test section assembly of the X3 expansion tube. In red, the new Mach 12 nozzle, sitting inside the new dump tank extension. In yellow the sealing surface of the nozzle. In blue, the present test section. Model sit usually in the central test section.

## Conclusion

The objective of this study is to develop new Mach 12 capability in the X3 expansion tube for M12REST engine scramjet testing. However, understanding of the behaviour of expansion tubes for high Mach number, high density, and low enthalpy scramjet remains incomplete. Additionally, no parametric study of the use of a secondary driver has been done previously.

An experimental study in the X2 expansion tube facility has been carried out to evaluate the acoustic effects in scramjet conditions and the general effectiveness of a secondary driver. Results have shown that, contrary to the theory, the use of a secondary driver did not increase the quality of the test flow in X2, introducing an undesirable positive gradient in the pressure traces. CFD analysis has shown partial agreement with the experimental results, but substantial discrepancies have been observed for conditions that included a secondary driver. The cause has been attributed to diaphragm opening process and interface mixing. It has been determined that it is currently impossible to evaluate the test flow noise numerically. Furthermore, it is also not possible to adequately establish the effect of the X2's smaller length scales on these phenomena. Future work will repeat these experiments with X3 where larger length scales are expected to eliminate the effects of a non-ideal flow processes on the noise and unsteadiness phenomena of interest.

A fully instrumented Mach 12 nozzle is being designed, integrating a series of changes that will extend the operational envelope of the X3 expansion tube. Other changes include a new lightweight piston, and a new dump tank extension. Instrumentation in the nozzle will include pressure transducers and heat transfer gauges, allowing for a better flow characterization.

## Acknowledgments

This research was undertaken with the assistance of resources from the National Computational Infrastructure (NCI), which is supported by the Australian Government. The authors also wish to thank the Australian Research Council and the Queensland Smart State Research Facilities Fund 2005 for support and funding.

## References

- [1] D. Preller and M. K. Smart, "Scramjets for Reusable Launch of Small Satellites," in *20th AIAA International Space Planes and Hypersonic Systems and Technologies Conference*, Glasgow, Scotland, 6 - 9 July 2015.
- [2] E. T. Curran, "Scramjet engines: the first forty years," *Journal of Propulsion and Power*, vol. 17, no. 6, pp. 1138-1148, 2001.
- [3] M. R. Tetlow and C. J. Doolan, "Comparison of Hydrogen and Hydrocarbon-Fueled Scramjet Engines for Orbital Insertion," *Journal of Spacecraft and Rockets*, vol. 44, no. 2, p. 365-373, Mar 2007.
- [4] M. Smart, "Scramjets," in *Advances on Propulsion Technology for High-Speed Aircraft*, Vols. Educational Notes RTO-EN-AVT-150, NATO Research & Technology Organisation, 2007, pp. 9-38.
- [5] L. J. Doherty, M. K. Smart and D. J. Mee, "Experimental Testing of an Airframe Integrated 3D Scramjet at True Mach 10 Flight Conditions," in *19th AIAA International Space Planes and Hypersonic Systems and Technologies Conference*, Atlanta, Georgia, USA, 16-20 June 2014.
- [6] D. Wise, "Experimental investigation of a three dimensional scramjet engine at hypervelocity conditions," University of Queensland, Brisbane, 2015.
- [7] J. E. Barth, "Mixing and combustion enhancement in a Mach 12 shape-transitioning scramjet engine," University of Queensland, Brisbane, 2014.
- [8] "Commercial Space Transportation Forecasts," Federal Aviation Administration - Commercial Space Transportation Advisory committee, 2015.
- [9] K. G. Bowcutt and T. R. Smith, "Responsive and Affordable Launch of Small Satellites: A reusable Air-breathing concept," in *AIAA Reinventing Space Conference*, Los Angeles, California, USA, 7 - 11 May 2012.
- [10] T. Jazra, D. Preller and M. K. Smart, "Design of an Airbreathing Second Stage for a Rocket-Scramjet-Rocket Launch Vehicle," *Journal of Spacecraft and Rockets*, vol. 50, no. 2, pp. 411-422, Mar 2013.
- [11] J. I. Erdos and R. J. Bakos, "Prospects for a quiet hypervelocity shock-expansion tunnel," in *25th Plasmadynamics and Lasers Conference*, Colorado Springs, Colorado, USA, 20 June 1994.
- [12] M. K. Smart, "Design of Three-Dimensional Hypersonic Inlets with Rectangular-to-Elliptical Shape Transition," *Journal of Propulsion and Power*, vol. 15, no. 3, p. 408-416, May 1999.
- [13] M. V. Suraweera and M. K. Smart, "Shock-Tunnel Experiments with a Mach 12 Rectangular-to-Elliptical Shape-Transition Scramjet at Offdesign Conditions," *Journal of Propulsion and Power*, vol. 25, no. 3, p. 555-564, May 2009.

- [14] L. Doherty, "An experimental investigation of an airframe integrated three-dimensional scramjet engine at a Mach 10 flight condition," University of Queensland, Brisbane, 2014.
- [15] M. Holden, "Studies of scramjet performance in the LENS facilities," in *36th AIAA/ASME/SAE/ASEE Joint Propulsion Conference and Exhibit*, Las Vegas, Nevada, USA, 17 - 19 July 2000.
- [16] M. Takahashi, T. Komuro, K. Sato, M. Kodera, H. Tanno and K. Itoh, "Effect of Combustor Shape on Scramjet Characteristics at Hypervelocity Condition over Mach 10 Flight," in *International Space Planes and Hypersonic Systems and Technologies Conferences*, Canberra, Australia, 6 -9 November 2006.
- [17] R. G. Morgan, "Chapter 4.2 - Shock Tubes and Tunnels: Facilities, Instrumentation, and Techniques," in *Handbook of Shock Waves*, G. Ben-Dor, O. Igra and T. Elperin, Eds., Burlington, Academic Press, 2001, pp. 587-601.
- [18] M. P. Scott, "Development and modelling of expansion tubes," University of Queensland, Brisbane, 2007.
- [19] M. McGilvray, R. M. Kirchhartz and T. Jazra, "Comparison of Mach 10 Scramjet Measurements from Different Impulse Facilities," *AIAA Journal*, vol. 48, no. 8, pp. 1647-1651, Aug 2010.
- [20] J. Sancho Ponce, "Scramjet testing at high total pressure," University of Queensland, Brisbane, 2015.
- [21] R. G. Morgan and R. J. Stalker, "Double diaphragm driven free piston expansion tube," in *Shock waves; Proceedings of the 18th International Symposium*, Sendai, Japan, 21 - 26 July 1991.
- [22] M. McGilvray, "Scramjet testing at high enthalpies in expansion tube facilities," University of Queensland, Brisbane, 2008.
- [23] R. L. Trimpi, "A preliminary theoretical study of the expansion tube: a new device for producing high-enthalpy short-duration hypersonic gas flows," 1962.
- [24] C. Miller, "Operational Experience in the Langley Expansion Tube With Various Test Gases," *NASA Technical Memorandum 78637*, 1977.
- [25] A. Paull and R. J. Stalker, "Test flow disturbances in an expansion tube," *Journal of Fluid Mechanics*, vol. 245, no. 1, pp. 493-521, 1992.
- [26] B. Henshall, "The Use of Multiple Diaphragms in Shock Tubes," *A.R.C. Technical Report C.P. No. 291. Ministry of Supply, Aeronautical Research Council*, 1956.
- [27] R. J. Stalker and D. Plumb, "Diaphragm-type Shock Tube for High Shock Speeds," *Nature*, vol. 218, no. 5143, pp. 789-790, May 1968.
- [28] D. E. Gildfind, C. M. James, P. Toniato and R. G. Morgan, "Performance considerations for expansion tube operation with a shock-heated secondary driver," *Journal of Fluid Mechanics*, vol. 777, pp. 364-407, Jul 2015.
- [29] R. G. Morgan, "Chapter 4.3 - Shock Tubes and Tunnels: Facilities, Instrumentation, and Techniques," in *Handbook of Shock Waves*, G. Ben-Dor, O. Igra and T. Elperin, Eds., Burlington, Academic Press, 2001, pp. 603-622.
- [30] M. McGilvray, R. G. Morgan and P. A. Jacobs, "Scramjet experiments in an expansion tunnel: evaluated using a quasi-steady analysis technique," *AIAA journal*, vol. 48, no. 8, pp. 1635-1646, Aug 2010.
- [31] D. E. Gildfind, R. G. Morgan, P. A. Jacobs and M. McGilvray, "Production of High-Mach-Number Scramjet Flow Conditions in an Expansion Tube.," *AIAA Journal*, vol. 52, pp. 162-177, 2014.
- [32] R. J. Gollan and P. A. Jacobs, "About the formulation, verification and validation of the hypersonic flow solver Eilmer," *Int. J. Numer. Meth. Fluids*, vol. 73, no. 1, p. 19-57, Mar 2013.
- [33] D. E. Gildfind, C. M. James and R. G. Morgan, "Free-piston driver performance characterisation using experimental shock speeds through helium," *Shock Waves*, vol. 25, no. 2, p. 169-176, Jan 2015.
- [34] D. E. Gildfind, "Development of high total pressure scramjet flow conditions using the X2 expansion tube," University of Queensland, Brisbane, 2012.
- [35] R. J. Goozee, "Simulation of a Complete Shock Tunnel Using Parallel Computer Codes," University of Queensland, Brisbane, 2003.
- [36] M. a. S. M. a. M. R. Wegener, "Optical study of a light diaphragm rupture process in an expansion tube," *Shock Waves*, vol. 10, no. 3, pp. 167-178, 2000.
- [37] S. Gordon and B. McBride, "Computer Program for Calculation of Complex Chemical Equilibrium Compositions and Applications," *NASA Reference Publication 1311*, 1994.
- [38] P. Jacobs, "L1d: A computer program for the simulation of transient-flow facilities," University of Queensland, 1999.
- [39] M. McGilvray, P. A. Jacobs, R. G. Morgan, R. J. Gollan and C. M. Jacobs, "Helmholtz Resonance of Pitot Pressure Measurements in Impulsive Hypersonic Test Facilities," *AIAA Journal*, vol. 47, no. 10, p. 2430-2439, Oct 2009.

- [40] A. G. Dann, R. G. Morgan, D. E. Gildfind, C. M. Jacobs, M. McGilvray and Z. F., "Upgrade of the X3 Super-orbital Expansion Tube," in *18th Australasian Fluid Mechanics Conference*, Launceston, Tasmania, Australia, 3 -7 December 2012.
- [41] M. Davey, "A hypersonic nozzle for the X3 expansion tube," university of Queensland, Brisbane, 2006.
- [42] R. G. Morgan and D. E. Gildfind, "X3 reflected shock tunnel for extended flow duration," in *Asia-Pacific International Symposium on Aerospace Technology APISAT*, Shanghai, China, 24 - 26 September 2014.
- [43] D. E. Gildfind, R. G. Morgan and J. Sancho, "Design and commissioning of a new lightweight piston for the X3 Expansion Tube," in *29th International Symposium on Shock Waves*, Madison, WI, United States, 14 - 19 July 2015.
- [44] H. Wei, W. Y. K. Chan, P. A. Jacobs and R. G. Morgan, "Computational optimisation and analysis of a truncated hypersonic nozzle for X3 expansion tunnel.," in *Proceedings of the 19th Australasian Fluid Mechanics Conference.*, Melbourne, Australia, 7 - 11 December 2014.